Crystal structure and ligandability of the 14-3-3/pyrin interface

Biochemical and Biophysical Research Communications 651 (2023) 1–7

Contents lists available at ScienceDirect

Biochemical and Biophysical Research Communications

journal homepage: www.elsevier.com/locate/ybbrc

Crystal structure and ligandability of the 14-3-3/pyrin interface

Roxanne Lau [a], Michael M. Hann [b, **], Christian Ottmann [a, *]

[a] Laboratory of Chemical Biology, Department of Biomedical Engineering and Institute for Complex Molecular Systems, Technische Universiteit Eindhoven, Den Dolech 2, 5612 AZ, Eindhoven, the Netherlands
[b] GSK Medicines Research Centre, Stevenage, SG1 2NY, UK

ARTICLE INFO

Article history:
Received 23 January 2023
Received in revised form
2 February 2023
Accepted 3 February 2023
Available online 4 February 2023

Keywords:
Protein-protein interactions
Fragments
Molecular glues
Small-molecule drug discovery
X-ray crystallography

ABSTRACT

Overactivation of Pyrin is the cause of the inflammatory diseases Mediterranean Fever and Pyrin-associated autoinflammation with neutrophilic dermatosis (PAAND). Binding of 14-3-3 proteins reduces the pro-inflammatory activity of Pyrin, hence small molecules that stabilize the Pyrin/14-3-3 complex could convey an anti-inflammatory effect. We have solved the atomic resolution crystal structures of phosphorylated peptides derived from PyrinpS208 and PyrinpS242 – the two principle 14-3-3 binding sites in Pyrin - in complex with 14-3-3 and analyzed the ligandability of these protein-peptide interfaces by crystal-based fragment soaking. The complex between 14-3-3 and PyrinpS242 appears to be much more amenable for small-molecule binding than that of 14-3-3/PyrinpS208. Consequently, only for the 14-3-3/PyrinpS242 complex could we find an interface-binding fragment, validating protein crystallography and fragment soaking as a method to evaluate the ligandability of protein surfaces.

1. Introduction

Pyrin, named after the Greek word for fever, is a 781-amino acid protein that is encoded by the gene *MEFV* (Mediterranean fever) and is predominantly expressed in granulocytes, eosinophils, monocytes, and dendritic cells [1,2]. Pyrin is comprised of four domains and displays extended regions of intrinsic disorder (Fig. 1A). Activated Pyrin assembles to form an inflammasome that subsequently activates caspase-1 which generates a proteolytic fragment of gasdermin-D, that oligomerizes to form pores in plasma membranes [1,3]. Caspase-1 also cleaves pro-IL-1β and pro-IL-18 to produce the active forms of these proinflammatory cytokines that are released into the extracellular space through gasdermin-D pores [4]. These processes facilitate a necrotic type of cell death that is called pyroptosis [3,5], suggesting that the highly conserved Pyrin inflammasome has a crucial role in host innate immunity, plays an important role in systemic autoinflammatory disorders (SAID) [6,7] and possibly might participate in the pathogenesis of other inflammatory diseases, like systemic-onset juvenile idiopathic arthritis [8].

In 2005, Jeru et al. reported 14-3-3 proteins as the direct binding partner of Pyrin as identified by a yeast-hybrid screen, with S208 and S242 as essential for the 14-3-3/Pyrin interaction, resulting in cytoplasmic localization of the complex [9]. 14-3-3 proteins are phosho-serine/threonine reader proteins that among other diseases play an important role in inflammation [10]. In 2016, Park et al. reported that the RhoA-dependent protein kinases PKN1 and PKN2 phosphorylate Pyrin at positions S208 and S242 [11], resulting in an interaction of Pyrin with 14-3-3. When complexed with 14-3-3, Pyrin remains in an inactivate state and does not engage in the formation of an active inflammasome. When RhoA is inactivated by bacterial toxins, PKN1 and PKN2 activity is reduced and levels of phosphorylated Pyrin are low. This prevents inhibitory 14-3-3 binding to Pyrin, promoting the formation of an active Pyrin inflammasome. This mechanism was confirmed by experiments in murine bone marrow-derived macrophages (BMDMs) and dendritic cells [12]. The important regulatory role of 14-3-3 binding to Pyrin was also strongly confirmed by the description of the dominantly inherited disorder called Pyrin-associated autoinflammation with neutrophilic dermatosis (PAAND) [13,14]. In PAAND, mutations of Pyrin at position 242 (S242A) or 244 (E244K) prevent PKN-mediated phosphorylation of Pyrin and consequently its binding to 14-3-3. Overexpression of S242A or E244K mutated proteins in HEK293T or THP1 cells resulted in increased inflammatory cell death suggesting constitutive activation of Pyrin. In HEK293T cells

* Corresponding author.
** Corresponding author.
E-mail address: c.ottmann@tue.nl (C. Ottmann).

https://doi.org/10.1016/j.bbrc.2023.02.013

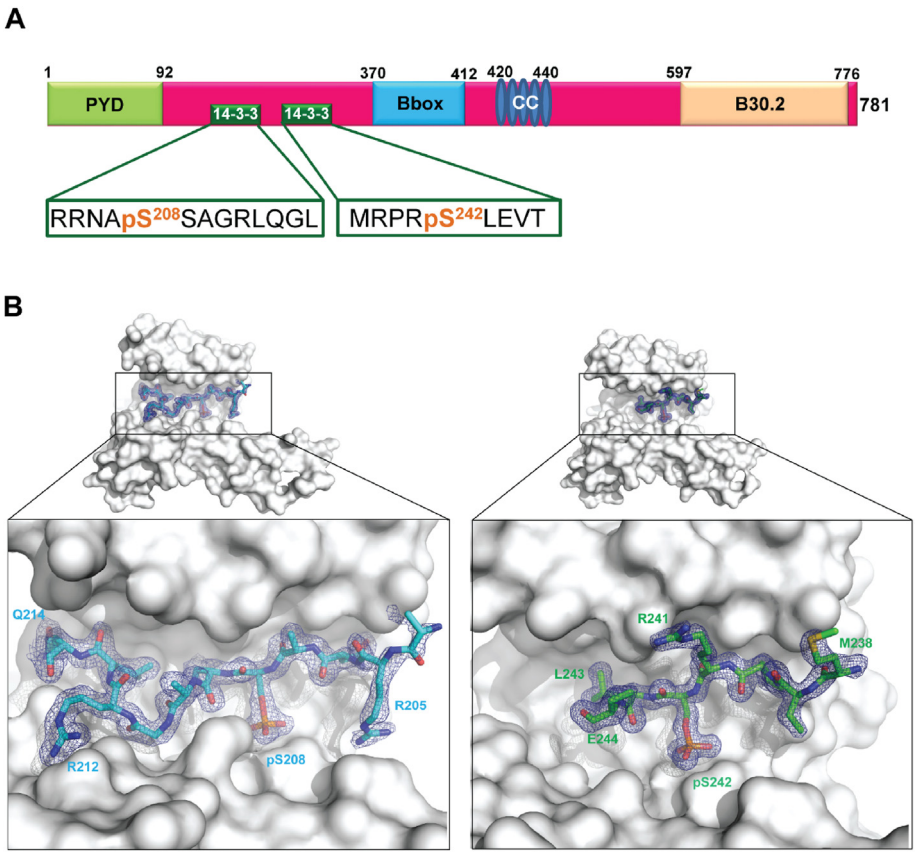

Fig. 1. Crystal structure of 14-3-3σ in complex with PyrinpS208 and PyrinpS242. (A) Domain structure of Pyrin with its Pyrin (PYD)-, Bbox-, Coiled-Coil (CC)-, and B30.2 domain as well as position and sequence of the two 14-3-3 binding sites. (B) Electron density maps (final 2Fo-Fc, contoured at 1σ) of PyrinpS208 (blue sticks) or PyrinpS242 (green sticks) bound to 14-3-3σ (white surface). (For interpretation of the references to color in this figure legend, the reader is referred to the Web version of this article.)

expressing wildtype or mutated Pyrin found in Familial Mediterranean Fever (FMF) patients, binding of inhibitory 14-3-3 to human mutant Pyrin was substantially reduced relative to binding to wt Pyrin [11]. Hong et al. showed in 2019 that mutations in the second 14-3-3 binding site (S208T, S208C) also cause familial autoinflammation [15]. Taken together, both the inhibitory effect on wt Pyrin as well its loss in clinically observed Pyrin mutants, suggests that stabilizing the binding of 14-3-3 to Pyrin could convey an anti-inflammatory, potentially therapeutically-useful effect. Enhancing this regulatory mechanism could, for example, be interesting in situation with acute or excessive activation of Pyrin (e.g. by the toxin TcdB produced by *Clostridium difficile*) that can lead to pathogenic inflammation [16].

We report here the crystal structures of both known 14-3-3 binding sites of Pyrin (pS208 and pS242), individually in complex with 14-3-3σ and the bivalent peptide encompassing both binding sites (pS208pS242) in complex with 14-3-3σ with high resolution (2.21 Å, 1.46 Å, and 1.63 Å, respectively). Visual inspection of the structures reveal likely significant differences in the 'ligandability' of the Pyrinps208 and PyrinpS242 site in complex with 14-3-3: while the peptide encompassing PyrinpS208 occupies the entire length of the 14-3-3 binding groove and forms no deeper composite interface pockets with 14-3-3, the PyrinpS242/14-3-3 interface shows a potentially more amenable pocket formed by residues of Pyrin C-terminal of pS242 and 14-3-3. Accordingly, soaking of fragment cocktails into crystals of the 14-3-3/PyrinpS208 complex didn't result in the identification of fragments binding to the protein/peptide interface, whereas we did identify a fragment that bound to the aforementioned pocket in the 14-3-3/PyrinpS242 interface. This ternary crystal structure with a resolution of 1.44 Å shows how the fragment engages the composite binding pocket formed by both the protein and the peptide, establishing contacts both to 14-3-3 and PyrinpS242.

2. Materials and methods

2.1. Protein expression and purification

14-3-3 protein was recombinantly expressed in BL21(DE3) cells using the pPROEX HTb vector encoding for the 14-3-3σΔC (ΔC17 truncated C-terminus) in TB medium. At a culture density of OD_{600} = 0.8–1, protein expression was initiated with 0.4 mM IPTG for 18 h at 18 °C. The cells were isolated by centrifugation (10.000 g, 15 min) and resuspended in lysis buffer (50 mM Tris/HCl pH8, 300 mM NaCl, 12.5 mM imidazole, 2 mM β-mercaptoethanol). A homogenizer was utilized for cell lysis, followed by centrifugation (40.000 g, 30min) to clear the lysate. The proteins were purified using standard protocols for Ni-NTA-columns. The protein was eluted with 250 mM imidazole (50 mM Tris/HCl pH8, 300 mM NaCl, 250 mM imidazole, 2 mM β-mercaptoethanol) and stored at −80 °C. The 14-3-3σΔC for crystallography required removal of the His6-tag by TEV protease; the TEV was removed with Ni-NTA-columns. To ensure highest purity, the 14-3-3σΔC was applied to a size exclusion chromatography (20 mM HEPES pH7.5, 150 mM NaCl, 2 mM β-mercaptoethanol) and stored at −80 °C.

Crystallography. The 14-3-3σ protein was C-terminally truncated (ΔC) after T231 to enhance crystallization. The 14-3-3 protein and Pyrin phosphopeptides PyrinpS208, PyrinpS242 as well as the

double-phosphorylated PyrinpS208pS242 were dissolved in complexation buffer (25 mM HEPES pH 7.5, 2 mM $MgCl_2$, 2 mM beta-mercaptoethanol (βME)) and mixed in a 1:2 M stoichiometry (protein:peptide, PyrinpS208 and PyrinpS242) or 1:0.5 (PyrinpS208pS242) at a final protein concentration of 12.5 mg/mL (470 μM). The complex was set up for hanging-drop crystallization after 30 min incubation at 4 °C, in 0.19 M $CaCl_2$, 5% glycerol, 26% PEG 400, 0.095 M HEPES, pH 7.5 (PyrinpS208 and PyrinpS242) or 0.2 M sodium citrate, 20% PEG 3350, and 0.1 M BisTris propane, pH 8.5 (PyrinpS208pS242). Crystal soaks were performed by mixing 0.4 μL of 50 mM stock solutions in dimethyl sulfoxide (DMSO) in 3.6 μL mother liquor, which was then added to drops containing multiple crystals. For the JenaScience fragments, 30 μL of crystallization buffer was added to the reservoir, 0.5 μL crystallization buffer on dried fragments in the well, and crystals were transferred into the fragment drop for overnight incubation. Soaked crystals were fished after overnight incubation at 4 °C and flash-cooled in liquid nitrogen. X-ray diffraction (XRD) data were collected either in-house on a Rigaku Compact HomeLab (equipped with Rigaku MicroMax-003 sealed tube X-ray source and Rigaku Dectris PILATUS3 R 200K detector, the Diamond Light Source or DESY PETRA III.

Initial processing was done using DIALS [17] in ccp4 [18] for datasets collected at DESY. The structures were phased by limited molecular replacement, using protein data bank (PDB) entry 4JC3 as a template, in Phaser [19]. Refmac5 from CCP4 was used for initial refinement as well as the cycles of refinement [20]. The presence of soaked fragments was verified by visual inspection of the Fo-Fc and 2Fo-Fc electron density maps in Coot [21]. Structure and restraints were generated using eLBOW [22] for successfully soaked ligands before using phenix.refine [23] and Coot in alternating cycles for model building and refinement. See Tables S1–S4 for XRD data collection, structure determination, and refinement statistics. Crystallographic data were deposited in the Protein Data Bank (PDB).

3. Results

To structurally characterize the interface of Pyrin and 14-3-3, we started with co-crystallization trials of short, mono-phosphorylated peptides derived from the PyrinpS208 and PyrinpS242 motif. Since the C-terminus of 14-3-3 is disordered and thus hampers crystallization, a 14-3-3σ construct that lacks the C-terminal 18 amino acids (14-3-3σΔC) was used for co-crystallization. Synthetic peptides derived from the Pyrin sequence surrounding pS208 (^{202}RLRRNApS^{208}SAGRLQGLAGGA^{220}) and pS242 (^{237}KMRPRpS^{242}LEVTIS^{248}) were individually complexed with 14-3-3σΔC in a 14-3-3/peptide ration of 1.5 and set-up for crystallization at a concentration of 12 mg/ml. Crystals of both complexes grew in 0.19 M $CaCl_2$, 5% glycerol, 26% PEG 400, 0.095 M HEPES, pH 7.5 and belonged to the space group C2221 with one 14-3-3σ monomer in the asymmetric unit. In the structure of 14-3-3σ in complex with the PyrinpS208 peptide 11 out of 19 residues were visible in the electron density (Fig. 1A and B). For the PyrinpS242 peptide 7 out 12 (238–246) residues could be built into the electron density (Fig. 1A and B).

The PyrinpS208 peptide occupies the entire length of the 14-3-3 binding channel (Fig. 2) and displays one of the most extensive 14-3-3/peptide interfaces known, comparable to the structures of 14-3-3 in complex with YAPpS127 [24], AtaxinpS776 [25] or LRRK2pS910 [26]. As with all phospho-dependent 14-3-3 protein-protein interactions the most prominent feature is the accommodation of the peptide's phosphate by 14-3-3's R56, R129 and Y130. In contrast to a number of other structurally described 14-3-3/peptide interactions – including PyrinpS242 (see below) – K49 is not participating in binding the phosphate, but rather engages in a

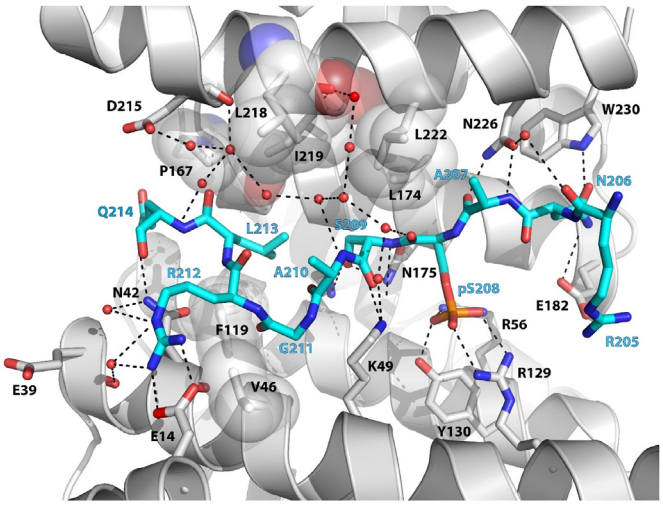

Fig. 2. Contacts between 14-3-3σ (white cartoon and sticks) and PyrinpS208 (blue sticks). Polar contacts are depicted by dashed lines, hydrophobic interactions are indicated by semi-transparent spheres of residues involved from 14-3-3σ. Water molecules are shown as red spheres. (For interpretation of the references to color in this figure legend, the reader is referred to the Web version of this article.)

main-chain contact with Pyrin's S209 carbonyl oxygen (Fig. 2). Different from the majority of 14-3-3 binding motifs of partner proteins, the PyrinpS208 peptide is not exiting the 14-3-3 binding channel C-terminal of the phosphorylated residue, but folds back and continues to occupy the entire length of the 14-3-3 binding groove. This seems to be mainly driven by two anchoring points, the salt-bridge between R212 of Pyrin and E14 of 14-3-3 and the way the hydrophobic side chain of L213 nestles into the hydrophobic environment of the back wall of the 14-3-3 binding channel (Fig. 2). The positioning of L213 is further supported by the peptide's main chain arrangement stabilized by a water-mediated contact of PyrinQ214's main-chain nitrogen with 14-3-3's D215 and the direct polar interaction of PyrinQ214's main-chain carbonyl with the side-chain nitrogen of N42 from 14-3-3 (Fig. 2). At the N-terminal of pS208, a number of specific contacts between the PyrinpS208 peptide and 14-3-3 are established. The side chain of R205 engages in a polar contact with the carboxyl group of 14-3-3's E182 side chain, while Pyrin's N206 interacts with both the ring-nitrogen in 14-3-3's W230's side chain and the carboxyl group of 14-3-3's E182 (Fig. 2). These interactions are complemented by a conserved main-chain contact with the peptide residue directly N-terminally preceding the phosphorylated amino acid (here A207) and the side chain of N226 of 14-3-3 (Fig. 2).

The PyrinpS242 peptide engages slightly less extensively with 14-3-3 compared to the PyrinpS208 site. As mentioned above, K49 together with R56, R129 and Y130 of 14-3-3 coordinate the phosphate moiety of PyrinpS242. The side chain of L243 of PyrinpS242 establishes hydrophobic contacts with L218, I219, and L222 of 14-3-3, respectively, and R239 and R241 of Pyrin engages in polar contacts with 14-3-3's D225 and E182 (Fig. 3).

Since the two 14-3-3 bindings sites in Pyrin are sufficiently close, we subsequently solved the structure of 14-3-3σ in complex with a 41-mer pyrin peptide containing both the pS208 and the pS242 site including the native sequence as linker between these sites. A broad screening resulted in crystals produced under the conditions of 0.2 M sodium citrate, 20% PEG 3350, and 0.1 M BisTris propane (pH 8.5). Initial growing of these crystals took several months, but streak-seeding techniques resulted in large crystals that only took a few days to grow. The structure was solved to 1.63 Å resolution with 2 copies of the 14-3-3 monomer in the asymmetric

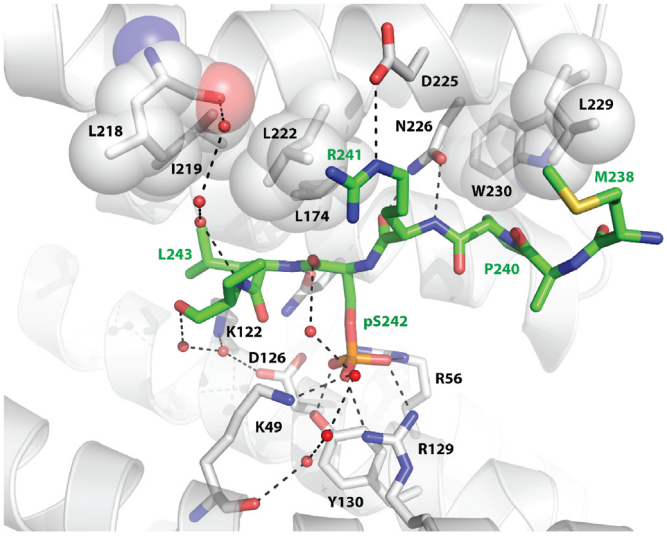

Fig. 3. Contacts between 14-3-3σ (white cartoon and sticks) and PyrinpS242 (green sticks). Polar contacts are depicted by dashed lines, hydrophobic interactions are indicated by semi-transparent spheres of residues involved from 14-3-3σ. Water molecules are shown as red spheres. (For interpretation of the references to color in this figure legend, the reader is referred to the Web version of this article.)

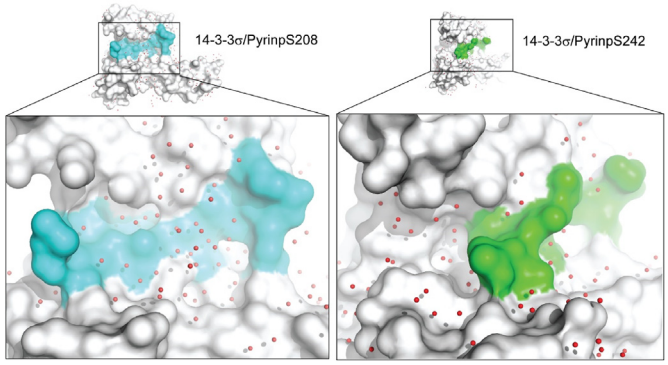

Fig. 5. Comparison of the protein-peptide interface of PyrinpS208 (blue surface) and PyrinpS242 (green surface) bound to 14-3-3σ (white surface). Water molecules are shown as red spheres. While the 14-3-3σ/PyrinpS208 interface is relatively featureless, the 14-3-3σ/PyrinpS242 complex creates a pocket for potential small -molecule binders. (For interpretation of the references to color in this figure legend, the reader is referred to the Web version of this article.)

unit that make up the physiological dimer. The structure was found to belong to the space group P21212 and both phosphorylated sites could be located in the structure (Fig. 4A). Of the 41 amino acids comprising the PyrinpS208pS242 peptide, 11 residues (205–2015) can be built into the electron density at the pS208 site, whereas 8

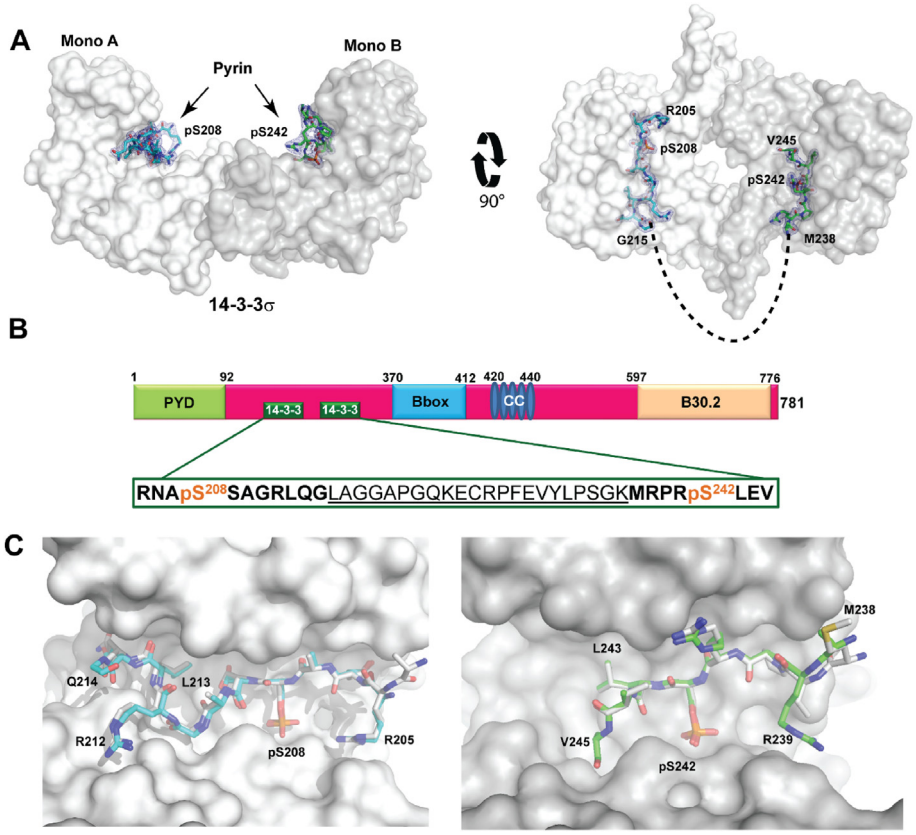

Fig. 4. Crystal structure of 14-3-3σ in complex with the di-phosphorylated peptide PyrinpS208pS242. (A) Electron density maps (final 2Fo-Fc, contoured at 1σ) of PyrinpS208 (blue sticks) and PyrinpS242 (green sticks) bound to a 14-3-3σ dimer (white and grey surface). The part of the peptide not visible in the electron density is represented by a dotted line. (B) Domain structure of Pyrin with its Pyrin (PYD)-, Bbox-, Coiled-Coil (CC)-, and B30.2 domain as well as the sequence of the di-phosphorylated PyrinppS208pS242 peptide. The residues visible in the electron are shown in bold, the residues not visible in the electron density are underlined. (C) Superimposition of the single peptide crystal structures of PyrinpS208 (white sticks, left) or PyrinpS242 (white sticks, right) with the respective sites in the PyrinpS208pS242 bivalent structure (color coding as in A). (For interpretation of the references to color in this figure legend, the reader is referred to the Web version of this article.)

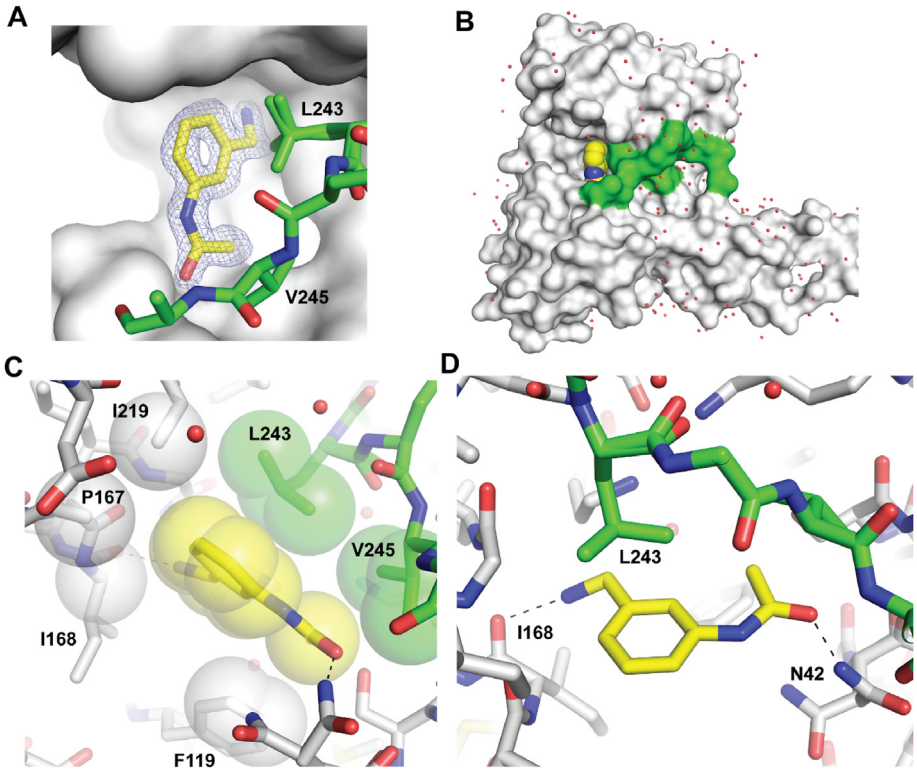

Fig. 6. Crystal structure of 14-3-3σ in complex with PyrinpS242 and a fragment identified from the Jena Biosciences fragment library. (A) Electron density maps (final 2Fo-Fc, contoured at 1σ) of Frag1 (blue sticks) and PyrinpS242 (green sticks) bound to 14-3-3σ (white surface). (B) Surface representation of the interface pocket between 14-3-3σ (white) and PyrinpS242 (green) to which Frag1 (yellow van-der-Waals spheres) binds. Crystallographic water molecules are shown as red spheres. (C) Hydrophobic contacts between Frag1 (yellow sticks and semi-transparent spheres), 14-3-3σ (white sticks and semi-transparent spheres), and PyrinpS242 (green sticks and semi-transparent spheres). (D) Polar contacts (dashed black line) between Frag1 (yellow sticks), 14-3-3σ (white sticks) and PyrinpS242 (green sticks). (For interpretation of the references to color in this figure legend, the reader is referred to the Web version of this article.)

residues (238–245) can be built into the electron density at the pS242 site (Fig. 4A). No electron density of the native sequence linking the two phosphorylation sites (Fig. 4B) could be identified, probably due to the retainment of high flexibility. Of the residues visible in the electron density, the positions of both main and side chains are nearly identical with the structures solved with the monovalent PyrinpS208 and PyrinpS242. The only exception is seen with R239 which is flipping its position in the 14-3-3 binding channel (Fig. 4C).

The analysis of the structures of 14-3-3 in complex with PyrinpS208 and PyrinpS242 revealed substantial differences in the architecture of the protein/peptide interfaces (Fig. 5). The PPI interface of the 14-3-3/PyrinpS208 complex is relatively featureless in the way of interesting pockets and thus likely offers only limited opportunities for ligands to bind (Fig. 5). In particular, the Fusicoccin-binding pocket – accessible in many other 14-3-3/peptide complexes like those with CRaf [27,28], Gab2 [29], CFTR [30], TASK3 [31], and p65 [32] - near the +1 amino acid position is occupied entirely by the C-terminal part of the PyrinpS208 peptide. Three other positions where we have previously found fragments – covalent fragments binding to Lys122 [33–35] and (engineered) Cys42 [36,37] as well as non-covalent amidine derivatives binding to Glu14 [38] – are also not accessible in the 14-3-3σ/PyrinpS208 structure. This evaluation of challenging ligandability of this interface was confirmed by the lack of hits from the extensive fragment cocktail soaks that we have carried out with a GSK fragment library of ca. 200 compounds designed for X-ray screening and the Frag Xtal Screen from Jena Bioscience (96 fragments). Although additional electron density was found in some of the soaked crystals, none of these were located at the central binding channel or near the peptide.

The protein/peptide interface looks substantially different in case of the 14-3-3/PyrinpS242 complex (Fig. 5). While the PyrinpS208 peptide occupies the entire length of the 14-3-3 binding channel and produces a more flat interface, the PyrinpS242 peptide occupies only around half of the length of the binding groove and produces a deeper, more extensive interface pocket that might be more 'ligandable'. While unfortunately fragment cocktail soaking with the GSK library didn't produce any hits, the idea of a more addressable pocket was confirmed by a hit from the fragment screen with the Jena Bioscience library (Fig. 6A). This fragment, (N-[3-(aminomethyl)phenyl]acetamide), was identified to bind in the direct vicinity of the +1 residue of PyrinpS242 (L243, Fig. 6A) and nestling in a pocket formed by the 14-3-3 binding groove and the peptide (Fig. 6B). The fragment makes 2 polar contacts with 14-3-3, one between the methylamine and the carbonyl oxygen of I168, the other with the OH group at the opposite site of the molecule and the side chain of N42 (Fig. 6C). Interactions with the PyrinpS242 peptide are of hydrophobic nature, both involving the side chain of L243 and V245. The latter makes a 30° turn to engage the fragment more intimately (Fig. 6D). This accommodation also moves T246 and the further C-terminus of the peptide, which is not visible in the density, out of the way to make place for the fragment (Fig. 6D).

4. Discussion

Fragment-based ligand discovery (FBLD) is enjoying continuous and increasing popularity for the identification of initial chemical matter in many drug discovery projects. One big advantage of FBLD is the rapid and cost-effective validation of the 'ligandability' of a

protein target. The 14-3-3s are a class of Ser/Thr-phosphorylation reader proteins that interact with hundreds of partner proteins in human cells. They bind to short, phosphorylated and intrinsically disordered linear peptide sequences within their partner proteins and induce a disorder-to-order transition in their partners, involving typically up to 15 amino acids of the 14-3-3 client protein. How these residues fold into the binding channel of the W-shaped 14-3-3 dimer can be very different among partner proteins [39]. For example, so-called mode-3 binding partners of 14-3-3 proteins interact via a sequence where the C-terminal, penultimate residue is the phosphorylated serine or threonine. The potassium channel TASK3 [31], the estrogen receptor ERα [40], the G protein RND3 [41] and the protein kinase DAPK2 [42] have been structurally characterized using such motifs to bind to 14-3-3. Since the phosphorylated S/T always binds to a highly conserved pocket roughly in the middle of the 14-3-3 binding channel, this mode-3 interaction leaves about half of the channel unoccupied. This allows for relatively large molecules like the natural product Fusicoccin A [31,40,42] and Pyrrolidone [43] to bind to this interface and stabilize the complex and was also the first example where a fragment tethering approach was shown to work [36]. A second type of 14-3-3 motifs leaves almost as much of the binding channel unoccupied as the mode 3 binders. This is achieved in their case by an at least 90° turn of the peptide main chain C-terminal of the +1 position, often facilitated by the presence of proline or glycine at the +2 and/or +3 position. These complexes are often also amenable to stabilization by natural products of the fusicoccane class, for example in the case of CRaf [28], Gab2 [29], CFTR [30], CaMKK2 [44] and p65 [32]. In addition, for such interfaces FBLD had been successful, by targeting complexes of 14-3-3 with p53 [38], p65 [33,34], Pin1 [35] and Amot-p130 [45].

A third class of binding modes is characterized by occupation of the peptide over the entire length of the 14-3-3 binding channel. As mentioned earlier, LRRKpS910 [26], AtaxinpS776 [25], YAPpS127/TAZpS89 [24,46], but also USP8pS718 [47] and SOS1pS1161 [48] belong to this category. In these cases, where the 'Fusicoccin pocket' is filled by the C-terminal part of the peptide, the composite surface is relatively featureless. Consequently, identifying small, orthosterically stabilizing molecules for these interfaces can be expected to be much more challenging than with 14-3-3 complexes of class 1 and 2. With the elucidation of the structures of two phosphomotifs from Pyrin binding to 14-3-3 one of which belongs to class 3 (PyrinpS208) and the other to class 2 (PyrinpS242), we saw the opportunity to perform a side-by-side comparison of the ligandability by fragment cocktail soaking of the respective co-crystals. While we could identify a fragment binding to the 14-3-3/PyrinpS242 interface, no fragments binding near the peptide were found in the 14-3-3/PyrinpS208 complex. This confirms the concept of differently chemistry-amenable 14-3-3 motifs, even when found in the same 14-3-3 partner protein. This is of relevance when evaluating a 14-3-3/client complex as a potential drug target, as many 14-3-3 partner proteins harbor more than one 14-3-3 binding site, ranging from examples with two like in Foxo1 [49], three like in p53 [50], four in LRRK2 [51,52] and up to nine in CFTR [53,54]. It is not entirely clear if stabilization of a given 14-3-3/partner protein complex via targeting different 14-3-3 binding motifs will result in different biological outcomes, since for the vast majority of 14-3-3 PPIs the effect of 14-3-3 binding on the target protein is described as the same, with just the overall binding affinity being influenced. If such differences are indeed of relevance, then this could be tested by specific stabilizers that target exclusively one of several 14-3-3 binding sites in a partner. As the results from this study indicate, identification of such site-specific binding moieties is possible.

Acknowledgements

We thank Jim Thorpe (Molecular Discovery, GSK) for assistance with interpretation of the crystallographic data and Emma Koppe (The GSK Immunology Network, Immunology Research Unit, GSK Stevenage) for therapeutic input. We thank the GSK Immunology Network, Immunology Research Unit, GSK Stevenage and the Dutch NWO (LIFT 731.016.406) for funding.

Appendix A. Supplementary data

Supplementary data to this article can be found online at https://doi.org/10.1016/j.bbrc.2023.02.013.

References

[1] O. Schnappauf, J.J. Chae, D.L. Kastner, I. Aksentijevich, The pyrin inflammasome in health and disease, Front. Immunol. 10 (2019) 1745, https://doi.org/10.3389/fimmu.2019.01745.
[2] R. Heilig, P. Broz, Function and mechanism of the pyrin inflammasome, Eur. J. Immunol. 48 (2018) 230–238, https://doi.org/10.1002/eji.201746947.
[3] J. Shi, Y. Zhao, K. Wang, X. Shi, Y. Wang, H. Huang, Y. Zhuang, T. Cai, F. Wang, F. Shao, Cleavage of GSDMD by inflammatory caspases determines pyroptotic cell death, Nature 526 (2015) 660–665, https://doi.org/10.1038/nature15514.
[4] S.M. Brewer, S.W. Brubaker, D.M. Monack, Host inflammasome defense mechanisms and bacterial pathogen evasion strategies, Curr. Opin. Immunol. 60 (2019) 63–70, https://doi.org/10.1016/j.coi.2019.05.001.
[5] J. Ding, K. Wang, W. Liu, Y. She, Q. Sun, J. Shi, H. Sun, D.-C. Wang, F. Shao, Pore-forming activity and structural autoinhibition of the gasdermin family, Nature 535 (2016) 111–116, https://doi.org/10.1038/nature18590.
[6] Y. Jamilloux, A. Belot, F. Magnotti, S. Benezech, M. Gerfaud-Valentin, E. Bourdonnay, T. Walzer, P. Sève, T. Henry, Geoepidemiology and immunologic features of autoinflammatory diseases: a comprehensive review, Clin. Rev. Allergy Immunol. 54 (2018) 454–479, https://doi.org/10.1007/s12016-017-8613-8.
[7] C.R. Harapas, A. Steiner, S. Davidson, S.L. Masters, An update on autoinflammatory diseases: inflammasomopathies, Curr. Rheumatol. Rep. 20 (2018) 40, https://doi.org/10.1007/s11926-018-0750-4.
[8] N.A. Ayaz, S. Ozen, Y. Bilginer, M. Ergüven, E. Taşkiran, E. Yilmaz, N. Beşbaş, R. Topaloğlu, A. Bakkaloğlu, MEFV mutations in systemic onset juvenile idiopathic arthritis, Rheumatology 48 (2009) 23–25, https://doi.org/10.1093/rheumatology/ken409.
[9] I. Jéru, S. Papin, S. L'hoste, P. Duquesnoy, C. Cazeneuve, J. Camonis, S. Amselem, Interaction of pyrin with 14.3.3 in an isoform-specific and phosphorylation-dependent manner regulates its translocation to the nucleus, Arthritis Rheum. 52 (2005) 1848–1857, https://doi.org/10.1002/art.21050.
[10] C.C. Munier, C. Ottmann, M.W.D. Perry, 14-3-3 modulation of the inflammatory response, Pharmacol. Res. 163 (2021), 105236, https://doi.org/10.1016/j.phrs.2020.105236.
[11] Y.H. Park, G. Wood, D.L. Kastner, J.J. Chae, Pyrin inflammasome activation and RhoA signaling in the autoinflammatory diseases FMF and HIDS, Nat. Immunol. 17 (2016) 914–921, https://doi.org/10.1038/ni.3457.
[12] W. Gao, J. Yang, W. Liu, Y. Wang, F. Shao, Site-specific phosphorylation and microtubule dynamics control Pyrin inflammasome activation, Proc. Natl. Acad. Sci. U. S. A. 113 (2016) E4857–4866, https://doi.org/10.1073/pnas.1601700113.
[13] S.L. Masters, V. Lagou, I. Jéru, P.J. Baker, L. Van Eyck, D.A. Parry, D. Lawless, D. De Nardo, J.E. Garcia-Perez, L.F. Dagley, C.L. Holley, J. Dooley, F. Moghaddas, E. Pasciuto, P.-Y. Jeandel, R. Sciot, D. Lyras, A.I. Webb, S.E. Nicholson, L. De Somer, E. van Nieuwenhove, J. Ruuth-Praz, B. Copin, E. Cochet, M. Medlej-Hashim, A. Megarbane, K. Schroder, S. Savic, A. Goris, S. Amselem, C. Wouters, A. Liston, Familial autoinflammation with neutrophilic dermatosis reveals a regulatory mechanism of pyrin activation, Sci. Transl. Med. 8 (2016) 332ra45, https://doi.org/10.1126/scitranslmed.aaf1471.
[14] F. Moghaddas, R. Llamas, D. De Nardo, H. Martinez-Banaclocha, J.J. Martinez-Garcia, P. Mesa-Del-Castillo, P.J. Baker, V. Gargallo, A. Mensa-Vilaro, S. Canna, I.P. Wicks, P. Pelegrin, J.I. Arostegui, S.L. Masters, A novel Pyrin-Associated Autoinflammation with Neutrophilic Dermatosis mutation further defines 14-3-3 binding of pyrin and distinction to Familial Mediterranean Fever, Ann. Rheum. Dis. 76 (2017) 2085–2094, https://doi.org/10.1136/annrheumdis-2017-211473.
[15] Y. Hong, A.S.I. Standing, S. Nanthapisal, N. Sebire, S. Jolles, E. Omoyinmi, R.H. Verstegen, P.A. Brogan, D. Eleftheriou, Autoinflammation due to homozygous S208 MEFV mutation, Ann. Rheum. Dis. 78 (2019) 571–573, https://doi.org/10.1136/annrheumdis-2018-214102.
[16] H. Xu, J. Yang, W. Gao, L. Li, P. Li, L. Zhang, Y.-N. Gong, X. Peng, J.J. Xi, S. Chen, F. Wang, F. Shao, Innate immune sensing of bacterial modifications of Rho GTPases by the Pyrin inflammasome, Nature 513 (2014) 237–241, https://doi.org/10.1038/nature13449.
[17] G. Winter, D.G. Waterman, J.M. Parkhurst, A.S. Brewster, R.J. Gildea, M. Gerstel,

L. Fuentes-Montero, M. Vollmar, T. Michels-Clark, I.D. Young, N.K. Sauter, G. Evans, DIALS: implementation and evaluation of a new integration package, Acta Crystallogr D Struct Biol 74 (2018) 85–97, https://doi.org/10.1107/S2059798317017235.

[18] M.D. Winn, C.C. Ballard, K.D. Cowtan, E.J. Dodson, P. Emsley, P.R. Evans, R.M. Keegan, E.B. Krissinel, A.G.W. Leslie, A. McCoy, S.J. McNicholas, G.N. Murshudov, N.S. Pannu, E.A. Potterton, H.R. Powell, R.J. Read, A. Vagin, K.S. Wilson, Overview of the CCP4 suite and current developments, Acta Crystallogr. D 67 (2011) 235–242, https://doi.org/10.1107/S0907444910045749.

[19] A.J. McCoy, R.W. Grosse-Kunstleve, P.D. Adams, M.D. Winn, L.C. Storoni, R.J. Read, Phaser crystallographic software, J. Appl. Crystallogr. 40 (2007) 658–674, https://doi.org/10.1107/S0021889807021206.

[20] G.N. Murshudov, P. Skubák, A.A. Lebedev, N.S. Pannu, R.A. Steiner, R.A. Nicholls, M.D. Winn, F. Long, A.A. Vagin, REFMAC5 for the refinement of macromolecular crystal structures, Acta Crystallogr D Biol Crystallogr 67 (2011) 355–367, https://doi.org/10.1107/S0907444911001314.

[21] P. Emsley, K. Cowtan, Coot: model-building tools for molecular graphics, Acta Crystallogr. D Biol. Crystallogr. 60 (2004) 2126–2132, https://doi.org/10.1107/S0907444904019158.

[22] N.W. Moriarty, R.W. Grosse-Kunstleve, P.D. Adams, Electronic Ligand Builder and Optimization Workbench (eLBOW): a tool for ligand coordinate and restraint generation, Acta Crystallogr D Biol Crystallogr 65 (2009) 1074–1080, https://doi.org/10.1107/S0907444909029436.

[23] P.D. Adams, P.V. Afonine, G. Bunkóczi, V.B. Chen, I.W. Davis, N. Echols, J.J. Headd, L.-W. Hung, G.J. Kapral, R.W. Grosse-Kunstleve, A.J. McCoy, N.W. Moriarty, R. Oeffner, R.J. Read, D.C. Richardson, J.S. Richardson, T.C. Terwilliger, P.H. Zwart, PHENIX: a comprehensive Python-based system for macromolecular structure solution, Acta Crystallogr. D Biol. Crystallogr. 66 (2010) 213–221, https://doi.org/10.1107/S0907444909052925.

[24] B. Schumacher, M. Skwarczynska, R. Rose, C. Ottmann, Structure of a 14-3-3σ-YAP phosphopeptide complex at 1.15 A resolution, Acta Crystallogr., Sect. F: Struct. Biol. Cryst. Commun. 66 (2010) 978–984, https://doi.org/10.1107/S1744309110025479.

[25] S. Leysen, R.J. Burnley, E. Rodriguez, L.-G. Milroy, L. Soini, C.J. Adamski, L. Nitschke, R. Davis, T. Obsil, L. Brunsveld, T. Crabbe, H.Y. Zoghbi, C. Ottmann, J.M. Davis, A structural study of the cytoplasmic chaperone effect of 14-3-3 proteins on ataxin-1, J. Mol. Biol. 433 (2021), 167174, https://doi.org/10.1016/j.jmb.2021.167174.

[26] L.M. Stevers, R.M.J.M. de Vries, R.G. Doveston, L.-G. Milroy, L. Brunsveld, C. Ottmann, Structural interface between LRRK2 and 14-3-3 protein, Biochem. J. 474 (2017) 1273–1287, https://doi.org/10.1042/BCJ20161078.

[27] C. Ottmann, M. Weyand, T. Sassa, T. Inoue, N. Kato, A. Wittinghofer, C. Oecking, A structural rationale for selective stabilization of anti-tumor interactions of 14-3-3 proteins by cotylenin A, J. Mol. Biol. 386 (2009) 913–919.

[28] M. Molzan, S. Kasper, L. Röglin, M. Skwarczynska, T. Sassa, T. Inoue, F. Breitenbuecher, J. Ohkanda, N. Kato, M. Schuler, C. Ottmann, Stabilization of physical RAF/14-3-3 interaction by cotylenin A as treatment strategy for RAS mutant cancers, ACS Chem. Biol. 8 (2013) 1869–1875, https://doi.org/10.1021/cb4003464.

[29] D. Bier, M. Bartel, K. Sies, S. Halbach, Y. Higuchi, Y. Haranosono, T. Brummer, N. Kato, C. Ottmann, Small-molecule stabilization of the 14-3-3/Gab2 protein-protein interaction (PPI) interface, ChemMedChem 11 (2016) 911–918, https://doi.org/10.1002/cmdc.201500484.

[30] L.M. Stevers, C.V. Lam, S.F.R. Leysen, F.A. Meijer, D.S. van Scheppingen, R.M.J.M. de Vries, G.W. Carlile, L.G. Milroy, D.Y. Thomas, L. Brunsveld, C. Ottmann, Characterization and small-molecule stabilization of the multisite tandem binding between 14-3-3 and the R domain of CFTR, Proc. Natl. Acad. Sci. U.S.A. 113 (2016) E1152–1161, https://doi.org/10.1073/pnas.1516631113.

[31] C. Anders, Y. Higuchi, K. Koschinsky, M. Bartel, B. Schumacher, P. Thiel, H. Nitta, R. Preisig-Müller, G. Schlichthörl, V. Renigunta, J. Ohkanda, J. Daut, N. Kato, C. Ottmann, A semisynthetic fusicoccane stabilizes a protein-protein interaction and enhances the expression of K+ channels at the cell surface, Chem. Biol. 20 (2013) 583–593, https://doi.org/10.1016/j.chembiol.2013.03.015.

[32] M. Wolter, P. de Vink, J.F. Neves, S. Srdanovic, Y. Higuchi, N. Kato, A.J. Wilson, I. Landrieu, L. Brunsveld, C. Ottmann, Selectivity via cooperativity: preferential stabilization of the p65/14-3-3 interaction with semi-synthetic natural products, J. Am. Chem. Soc. (2020), https://doi.org/10.1021/jacs.0c02151.

[33] M. Wolter, D. Valenti, P.J. Cossar, L.M. Levy, S. Hristeva, T. Genski, T. Hoffmann, L. Brunsveld, D. Tzalis, C. Ottmann, Fragment-based stabilizers of protein-protein interactions through imine-based tethering, Angew Chem. Int. Ed. Engl. (2020), https://doi.org/10.1002/anie.202008585.

[34] M. Wolter, D. Valenti, P.J. Cossar, S. Hristeva, L.M. Levy, T. Genski, T. Hoffmann, L. Brunsveld, D. Tzalis, C. Ottmann, An exploration of chemical properties required for cooperative stabilization of the 14-3-3 interaction with NF-κB-Utilizing a reversible covalent tethering approach, J. Med. Chem. 64 (2021) 8423–8436, https://doi.org/10.1021/acs.jmedchem.1c00401.

[35] P.J. Cossar, M. Wolter, L. van Dijck, D. Valenti, L.M. Levy, C. Ottmann, L. Brunsveld, Reversible covalent imine-tethering for selective stabilization of 14-3-3 hub protein interactions, J. Am. Chem. Soc. 143 (2021) 8454–8464, https://doi.org/10.1021/jacs.1c03035.

[36] E. Sijbesma, K.K. Hallenbeck, S. Leysen, P.J. de Vink, L. Skóra, W. Jahnke, L. Brunsveld, M.R. Arkin, C. Ottmann, Site-directed fragment-based screening for the discovery of protein-protein interaction stabilizers, J. Am. Chem. Soc. 141 (2019) 3524–3531, https://doi.org/10.1021/jacs.8b11658.

[37] E. Sijbesma, K.K. Hallenbeck, S.A. Andrei, R.R. Rust, J.M.C. Adriaans, L. Brunsveld, M.R. Arkin, C. Ottmann, Exploration of a 14-3-3 PPI pocket by covalent fragments as stabilizers, ACS Med. Chem. Lett. 12 (2021) 976–982, https://doi.org/10.1021/acsmedchemlett.1c00088.

[38] X. Guillory, M. Wolter, S. Leysen, J.F. Neves, A. Kuusk, S. Genet, B. Somsen, J. Morrow, E. Rivers, L. van Beek, J. Patel, R. Goodnow, H. Schoenherr, N. Fuller, Q. Cao, R.G. Doveston, L. Brunsveld, M.R. Arkin, M.P. Castaldi, H. Boyd, I. Landrieu, H. Chen, C. Ottmann, Fragment-based differential targeting of PPI stabilizer interfaces, J. Med. Chem. (2020), https://doi.org/10.1021/acs.jmedchem.9b01942.

[39] N.N. Sluchanko, Recent advances in structural studies of 14-3-3 protein complexes, Adv Protein Chem Struct Biol 130 (2022) 289–324, https://doi.org/10.1016/bs.apcsb.2021.12.004.

[40] I.J. De Vries-van Leeuwen, D. da Costa Pereira, K.D. Flach, S.R. Piersma, C. Haase, D. Bier, Z. Yalcin, R. Michalides, K.A. Feenstra, C.R. Jiménez, T.F.A. de Greef, L. Brunsveld, C. Ottmann, W. Zwart, A.H. de Boer, Interaction of 14-3-3 proteins with the estrogen receptor alpha F domain provides a drug target interface, Proc. Natl. Acad. Sci. U.S.A. 110 (2013) 8894–8899, https://doi.org/10.1073/pnas.1220809110.

[41] P. Riou, S. Kjær, R. Garg, A. Purkiss, R. George, R.J. Cain, G. Bineva, N. Reymond, B. McColl, A.J. Thompson, N. O'Reilly, N.Q. McDonald, P.J. Parker, A.J. Ridley, 14-3-3 proteins interact with a hybrid prenyl-phosphorylation motif to inhibit G proteins, Cell 153 (2013) 640–653, https://doi.org/10.1016/j.cell.2013.03.044.

[42] M. Horvath, O. Petrvalska, P. Herman, V. Obsilova, T. Obsil, 14-3-3 proteins inactivate DAPK2 by promoting its dimerization and protecting key regulatory phosphosites, Commun Biol 4 (2021) 986, https://doi.org/10.1038/s42003-021-02518-y.

[43] F. Bosica, S.A. Andrei, J.F. Neves, P. Brandt, A. Gunnarsson, I. Landrieu, C. Ottmann, G. O'Mahony, Design of drug-like protein-protein interaction stabilizers Guided by chelation-controlled bioactive conformation stabilization, Chemistry 26 (2020) 7131–7139, https://doi.org/10.1002/chem.202001608.

[44] D. Lentini Santo, O. Petrvalska, V. Obsilova, C. Ottmann, T. Obsil, Stabilization of protein-protein interactions between CaMKK2 and 14-3-3 by fusicoccins, ACS Chem. Biol. 15 (2020) 3060–3071, https://doi.org/10.1021/acschembio.0c00821.

[45] F. Centorrino, B. Andlovic, P. Cossar, L. Brunsveld, C. Ottmann, Fragment-based exploration of the 14-3-3/Amot-p130 interface, Curr Res Struct Biol 4 (2022) 21–28, https://doi.org/10.1016/j.crstbi.2021.12.003.

[46] E. Sijbesma, L. Skora, S. Leysen, L. Brunsveld, U. Koch, P. Nussbaumer, W. Jahnke, C. Ottmann, Identification of two secondary ligand binding sites in 14-3-3 proteins using fragment screening, Biochemistry 56 (2017) 3972–3982, https://doi.org/10.1021/acs.biochem.7b00153.

[47] F. Centorrino, A. Ballone, M. Wolter, C. Ottmann, Biophysical and structural insight into the USP8/14-3-3 interaction, FEBS Lett. 592 (2018) 1211–1220, https://doi.org/10.1002/1873-3468.13017.

[48] A. Ballone, F. Centorrino, M. Wolter, C. Ottmann, Structural characterization of 14-3-3ζ in complex with the human Son of sevenless homolog 1 (SOS1), J. Struct. Biol. 202 (2018) 210–215, https://doi.org/10.1016/j.jsb.2018.01.011.

[49] M. Saline, L. Badertscher, M. Wolter, R. Lau, A. Gunnarsson, T. Jacso, T. Norris, C. Ottmann, A. Snijder, AMPK and AKT protein kinases hierarchically phosphorylate the N-terminus of the FOXO1 transcription factor, modulating interactions with 14-3-3 proteins, J. Biol. Chem. (2019), https://doi.org/10.1074/jbc.RA119.008649.

[50] M. Falcicchio, J.A. Ward, S. Macip, R.G. Doveston, Regulation of p53 by the 14-3-3 protein interaction network: new opportunities for drug discovery in cancer, Cell Death Dis. 6 (2020) 126, https://doi.org/10.1038/s41420-020-00362-3.

[51] K. Muda, D. Bertinetti, F. Gesellchen, J.S. Hermann, F. von Zweydorf, A. Geerlof, A. Jacob, M. Ueffing, C.J. Gloeckner, F.W. Herberg, Parkinson-related LRRK2 mutation R1441C/G/H impairs PKA phosphorylation of LRRK2 and disrupts its interaction with 14-3-3, Proc. Natl. Acad. Sci. U.S.A. 111 (2014) E34–43, https://doi.org/10.1073/pnas.1312701111.

[52] J.T. Manschwetus, M. Wallbott, A. Fachinger, C. Obergruber, S. Pautz, D. Bertinetti, S.H. Schmidt, F.W. Herberg, Binding of the human 14-3-3 isoforms to distinct sites in the leucine-rich repeat kinase 2, Front. Neurosci. 14 (2020) 302, https://doi.org/10.3389/fnins.2020.00302.

[53] Z. Bozoky, M. Krzeminski, R. Muhandiram, J.R. Birtley, A. Al-Zahrani, P.J. Thomas, R.A. Frizzell, R.C. Ford, J.D. Forman-Kay, Regulatory R region of the CFTR chloride channel is a dynamic integrator of phospho-dependent intra- and intermolecular interactions, Proc. Natl. Acad. Sci. U.S.A. 110 (2013) E4427–4436, https://doi.org/10.1073/pnas.1315104110.

[54] L.M. Stevers, P.J. de Vink, C. Ottmann, J. Huskens, L. Brunsveld, A thermodynamic model for multivalency in 14-3-3 protein-protein interactions, J. Am. Chem. Soc. 140 (2018) 14498–14510, https://doi.org/10.1021/jacs.8b09618.